



Pseudo Dynamic Test and Time-History Analyses of Traditional-Style Steel Frame Structures

Liangjie Qi^{1,2} · Jianyang Xue¹

Received: 22 March 2017 / Accepted: 1 September 2017 / Published online: 25 April 2018
© Korean Society of Steel Construction 2018

Abstract

To study the seismic performances of steel frame structures in traditional-style buildings, the pseudo-dynamic test was carried out on a 1/2 ratio model built in the areas with a seismic design intensity of eight. The input earthquake waves included El Centro, Lanzhou and Wenchuan, and the maximum peak accelerations of these ground motions were 70, 200, 400 and 620 gal (0.7, 2, 4 and 6.2 m/s²). The seismic responses such as displacement, reaction force, acceleration were recorded. The hysteretic behavior, energy dissipation capacity, time-history curves of acceleration and displacement, bearing capacity and stiffness degradation were analyzed. The results show that the traditional-style steel frame structure stayed in the elastic stage subjected to no more than 400 gal (4 m/s²) PGA. There was no obvious pinch phenomenon in the hysteretic loops and the structural energy dissipation increased significantly with the increase of the seismic wave amplitude. When the 9-intensity seismic wave was applied, some unique members in traditional-style buildings yielded, and the spectral characteristic of the input seismic wave had a great influence on the seismic response of the structure. The modal analysis and time-history analyses were applied to the structure, the vertical deformation of the second and third modes of the steel frame was larger than that of the first modal shape, the reaction force value of finite element was a little larger than that of the test under the same loading condition. When the structure subjected to more severe earthquake, some unique members in traditional-style buildings acted as the first earthquake fortification line and dissipate most energy, and the structural most obvious reaction took place in advance or delayed a bit.

Keywords Traditional-style buildings · Steel frame structures · Pseudo-dynamic tests · Modal analysis · Time-history analyses · Seismic performance

1 Introduction

The ancient architecture embodies the Chinese history, science and technology, ancient culture, religion and other achievements, which give birth to a valuable national culture and spirit. However, ancient buildings are mostly made of timber (Fang et al. 2001), and the material has its own restrictions, such as easy warping, easy to decay and so on. The damage phenomenon, even collapse, of the existing wooden structure appears after suffering years of natural hazard (Wodzicki 2001). Therefore, using other new

materials to build the traditional-style buildings is fatal to inherit these historical architecture. The modern science and technology is applied in the traditional-style buildings, which enhances the disaster resistance significantly, and it has gradually integrated into the construction industry in various fields, especially widely used at the landmarks and landscape gardens (Tian 2010), such as Danfeng Gate in Daming Palace, Changan Tower and Dingding Gate of Luoyang City, which have become local landmark buildings. Figure 1 is a typical steel traditional-style structure. The external appearance is similar to that of ancient wooden buildings, which varies considerably with the common framework of the modern buildings. For example, the Dou-Gong components and large cornices are the most obvious difference. Due to the use of modern building materials, the joint connection pattern changes from mortise-tenon connection (wood) to weld or bolt connection (steel), and a huge difference appears in the force transfer characteristics

✉ Jianyang Xue
jianyang_xue@163.com

¹ Department of Civil Engineering, Xi'an University of Architecture and Technology, Xi'an 710055, China

² Department of Civil and Environmental Engineering, Virginia Tech, Blacksburg 24060, USA



Fig. 1 Typical steel traditional-style buildings

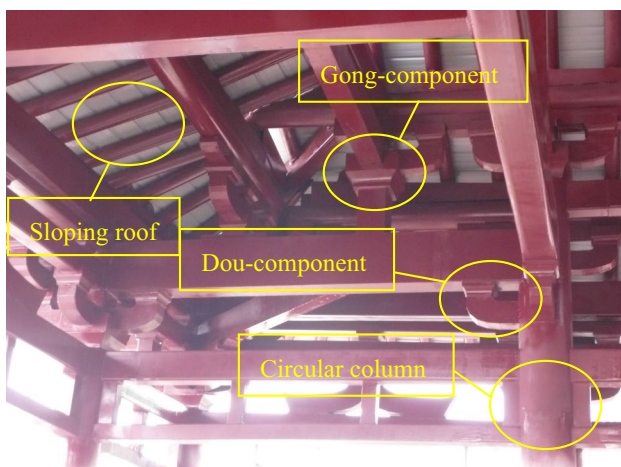


Fig. 2 Detailed construction

(Xue et al. 2015). Detailed constructions of traditional-style structure are illustrated in Fig. 2. These modern incarnations of ancient Chinese architectural styles will be called Traditional-style buildings (TSB) in this paper.

The researches on the frame structure system mainly focused on frame-braced structure, steel high-rise frame structures. Tremblay et al. (2003) described an experimental study on the seismic performance of concentrically braced steel frames made with cold-formed rectangular tubular bracing members, 24 quasi static cyclic tests were performed on full size X bracing and single diagonal bracing systems, the results clearly showed that the effective length of the braces can be used to determine their compression strength and to characterize their hysteretic response. Yang et al. (2017) investigated the seismic performance of reinforced concrete structures retrofitted with BRBs, quasi-static test of two single-bay and 3-story

reinforced concrete frames specimens was conducted and introduced, the results indicated that the specimen retrofitted with BRBs showed much better seismic performance than the control specimen without BRBs. Jan et al. (2004) put forward a new simplified pushover analysis procedure for high-rise buildings, and five different-height buildings were used as examples to illustrate the application of the proposed procedure. However, there were just a few researches investigating the seismic behavior of TSB. Xue and Qi (2016) experimentally investigated the behavior of steel frame structures of traditional-style buildings subjected to combined constant axial load and reversed lateral cyclic loading conditions. Test results showed that the Dou-Gong component in steel frame structures acted as the first seismic line under the action of horizontal loads, and satisfied the Chinese Seismic Design Principle of “strong columns-weak beams, strong joints-weak members”. Xue et al. (2016) designed four steel double beams-column interior joint models in 1/2 scale, the failure mode, hysteretic performance, and ductility of the joints were obtained from the pseudo-static experiment. There were 3 small core areas, namely an upper core area, a lower core area and a middle short column, appeared in the steel double-beams-column in the TSB during loading. And the failure mode of the double beams-column joint was the shear failure. Besides these, almost no other research has been conducted academically.

The unique layout of the sloping roof, circular columns, Dou-Gong and other special members in TSB make such kind of structure more complicated, and the design of such structure has not yet been involved in the current seismic specification. In the study of the seismic performance of steel frame structure, the man-made intervention during the quasi-static test is obvious at present (Tsai et al. 2008). The actual dynamic response can not be reflected exactly under quasi-static test. And the shake table test is greatly influenced by the size effect and other factors, resulting in higher distortion of test results. Therefore, the application of pseudo-dynamic test (PDT) is more and more extensive, it owns the merit of the simpleness of static test and applies the actual seismic waves to the structures, and is able to obtain the real structural response under the seismic dynamic effect (Lauriola and Sandhaas 2006).

In order to study the seismic performance of the TSB system subjected to earthquake wave, a typical TSB frame was designed and fabricated based on the study of the mechanical properties of the traditional-style abnormal joints (Xue et al. 2015, 2016), and the pseudo-dynamic test was carried out. The vibration mode of the structure was analyzed by finite element method, and the more severe seismic waves were applied to it, which could provide a reference to the design of such structures.

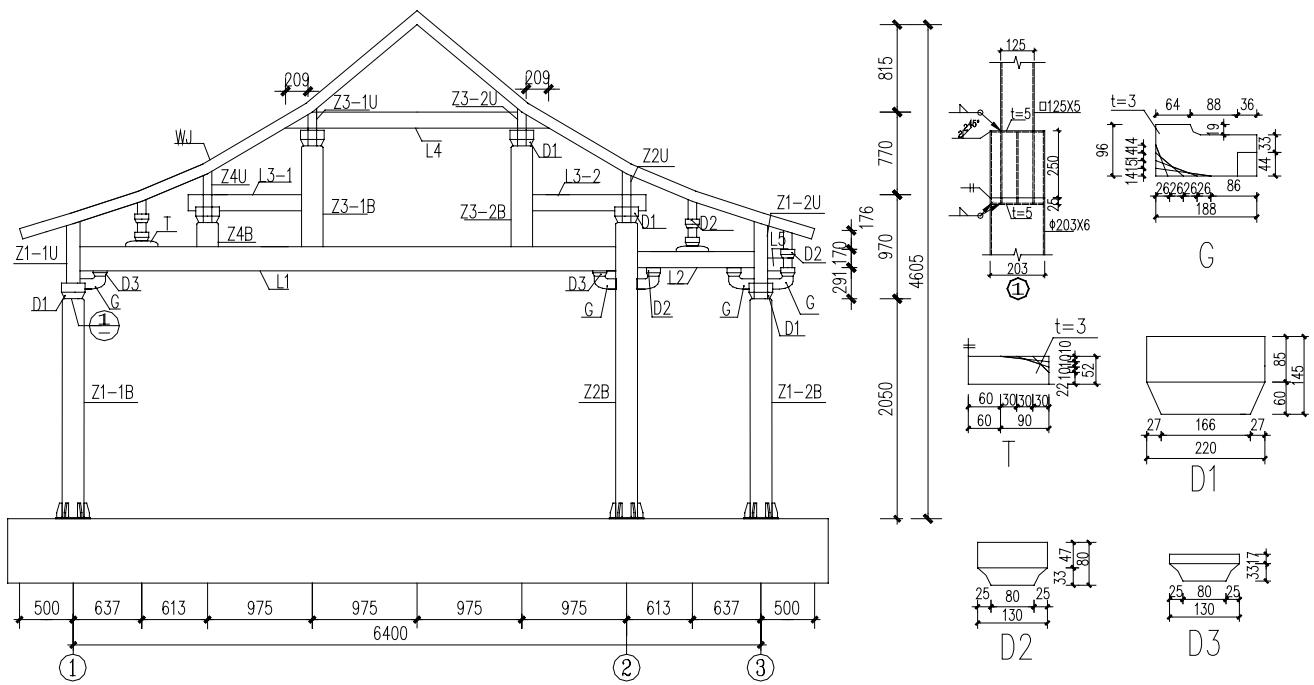


Fig. 3 Dimensions and details of specimens

2 Experimental Program

2.1 Specimen Design and Fabrication

The one-storey two-bay prototype structure was designed for a highly seismic location in China, the typical bay width was 12.8 m and the total height was 9.21 m. Due to the limitation of the test site, the scale ratio of the structure was taken as 1/2. After the fabrication of the model components in the factory, the assembling was taken on at the laboratory. The facade and detailed size are shown in Fig. 3, and the cross-sectional dimensions of the members are shown in Table 1. Apart from the column footing and the ground beam bolting together, the rest connection in the specimen were all welded. Six stiffening ribs were mounted at each column footing, in order to strengthen the moment resisting ability. Because of the space requirement of the traditional-style building, the main girder (L1), stretched across the main span, was 225 mm × 125 mm box-section. The side girder (L2), located at the side span, of 150 mm × 100 mm was welded box-section, forming an irregular joint with different height beams on each side. The steel grade was Q235B (nominal yield strength of 235 Mpa), and the E43 electrode was used for manual welding. The steel plate used for material coupon test was taken according to Steel and Steel Products-location and Preparation of Test Pieces for Mechanical Testing (GB/T2975-1998), whose results are displayed in Table 2.

Table 1 Member sizes

Component	Number	Cross-section size (mm)
Column	Z1-1B, Z1-2B, Z2B	φ203 × 6
	Z1-1U, Z1-2U	□125 × 5
	Z3-1B, Z3-2B, Z4B	□125 × 3
	Z2U, Z4U, Z3-1U, Z3-2U	□80 × 3
		□80 × 3
Beam	L1	□225 × 125 × 3
	L2, L3-1, L3-2, L4	□150 × 100 × 3
	L5	□120 × 100 × 3
Roof	WJ	□100 × 3

φ and □ represent the circular section and rectangular cross-section, respectively. The first or first two values of cross-section size mean the side length, the last number represents the sectional thickness

Table 2 Material properties of steel

Thickness, <i>t</i> (mm)	Yield strength, <i>f_y</i> (MPa)	Yield strain, <i>ε_y</i> (10 ⁻⁶)	Ultimate strength, <i>f_u</i> (MPa)	Ultimate strain, <i>E_s</i> (MPa)
3	327.3	1544	476.8	2.12 × 105
5	317.6	1557	390.7	2.04 × 105
10	289.2	1530	407.1	1.89 × 105
6	306.3	1612	362.6	1.90 × 105

In order to satisfy the mass and weight similarity between the test model and prototype (Zheng 2000), the roof distributed load was equivalent to the vertical concentrated load applied along the top of columns Z1-1B, Z3-1B, Z3-2B, ZB2, Z1-2B. Considering the sloping roof construction and the safety factors during the loading, the external load was hanged up using concrete block. On account of the site size, the length similarity coefficient was 1/2, and the other dynamic similarity coefficients are listed in Table 3.

2.2 Input Motion Selection

The prototype of this test model is located in the 8-intensity seismic area, the site category is class II. When choosing seismic waves, the predominant period of seismic waves should be close to the spectral characteristics of location as far as possible. Therefore, El Centro wave, Wenchuan wave and Lanzhou wave were chosen as the input ground motions of the PDTs and were scaled to represent 63, 10 and 2% probabilities of exceedence in 50 years’ seismic hazard levels (GB50011-2010). Among them, Lanzhou is an artificial wave and the other two are actual earthquake records. The original ground motion record is shown in Fig. 4. The mock-up was tested under eight conditions with different peak ground acceleration (PGA), and the acceleration amplitude was adjusted according to the similarity relation. At the

initial stage of the test, three kinds of seismic waves were input to observe the dynamic response of the TSB. When the plasticity of the structure appeared, only Wenchuan wave was input. The PGA of input seismic waves increased on the basis of frequent earthquake, moderate earthquake, rare earthquake of 8-intensity and rare earthquake of 9-intensity, respectively. The interval loading step is 0.014 s, the total of steps is 900 steps and the total time is 12.6 s.

2.3 Loading Scheme

The loading method of the test was based on “JGJ101-1996 Code for Seismic Testing of Buildings” and the loading was carried out at the Key Laboratory of Structural Engineering and Earthquake Resistance of Chinese Education Ministry. During the experiment, an MTS electro-hydraulic servo actuator was placed at the elevation of 2.420 m, and test data were collected and recorded by the TDS602 data acquisition. In order to prevent the instability out of the test plane, the two sides of the loading plane were supported by the pulley to ensure the stability of the structure (Baker and Charlton 1958). The overall frame model is shown in Fig. 5. Considering the actual distributed roof load and sloping roof, it is impossible to use jacks to apply the vertical load. In order to simulate the load case correctly, the concrete blocks were hanged up at each column top to substitute the distributed roof load. The weights of 7.8, 13.4, 9.4, 7.1 and 5.6 kN were applied to the Z1-1, Z3-1, Z3-2, Z2, Z1-2 column members, respectively. The initial stiffness was measured firstly, followed by the application of horizontal ground motion waves at the girder level to conduct PDTs. When loading, the ground fixers were used to fix the concrete foundation firstly. Then the vertical concrete masses were hung up at the separate columns. The initial small displacement loading was applied to the steel frame in order to reduce the distance between the actuator and the specimen, followed by the excitation of different seismic waves. The loading sequence is demonstrated in Table 4. As the specimen is a single-layer plane frame, the external load and the

Table 3 Dynamic similarities

Physical parameter	Relationship	Similarity coefficient
Length (L)	$S_L = L_m/L_p$	1/2
Displacement (X)	$S_X = S_L$	1/2
Seismic action (F)	$S_F = S_E S_L^2$	1/4
Time (t)	$S_t = [S_L S_\sigma / S_E]^{1/2}$	$1/\sqrt{2}$
Vertical stress (σ)	S_σ	1
Elastic modulus (E)	S_E	1
Input acceleration (S_{x_g})	$S_{x_g} = S_E / S_\sigma$	1

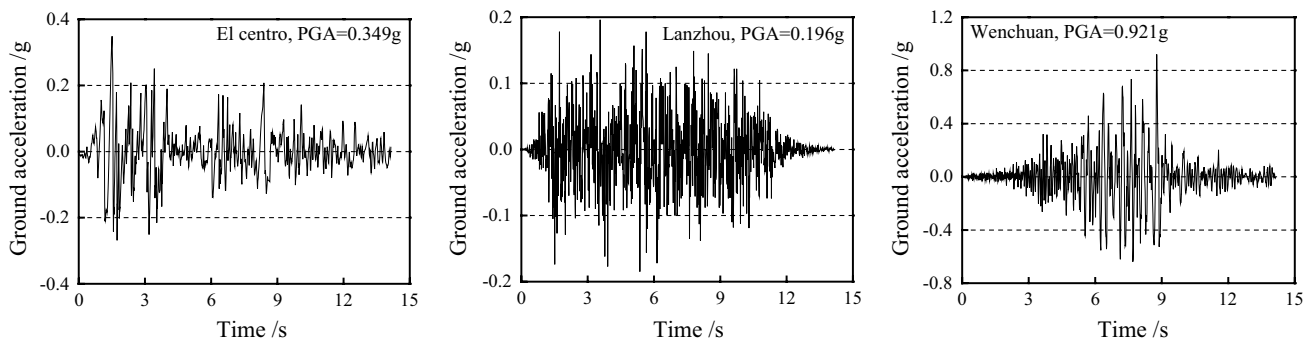


Fig. 4 Original ground accelerations (before scaling)



Fig. 5 Steel frame model

Table 4 PDTs loading system

No.	Wave	PGA (gal)	Seismic fortification intensity
1	El Centro	70	Frequent earthquake of 8-intensity
2	Lanzhou	70	Frequent earthquake of 8-intensity
3	Wenchuan	70	Frequent earthquake of 8-intensity
4	El Centro	200	Frequent earthquake of 8-intensity
5	Lanzhou	200	Moderate earthquake of 8-intensity
6	Wenchuan	200	Moderate earthquake of 8-intensity
7	Wenchuan	400	Rare earthquake of 8-intensity
8	Wenchuan	620	Rare earthquake of 9-intensity

self-weight of the structure are concentrated at the height of the actuator, then the total mass of the structure model is obtained, $M = 4863$ kg. In addition, according to the requirements of building seismic design specifications, the damping ratio of steel structure ζ equals to 0.04.

In addition to the placement of an MTS displacement transducer at the girder level, some more linear variable differential transducers (LVDTs) were installed at different elevations of the structure. To consider the effect of the horizontal and vertical displacements of the foundation during the experiment, a dial indicator was arranged at the end of the ground beam to detect its shift. The strain gauges were symmetrically arranged at each panel zone, beam end, column end and Dou-Gong component, respectively. The loading devices are shown in Fig. 6.

3 Experimental Results and Discussion

3.1 Experimental Observation

Under the seismic action with PGA of 70, 200 and 400 gal, the structural members all worked in the elastic working stage. No plastic deformation occurred and the bearing capacity was relatively high when subjected to the rare earthquake with no more than 8-intensity. When subjected to the wave whose PGA was 620 gal, yielding at the eastern bottom side of D1 component was detected, and then the yielding phenomenon occurred at the G component on the west side of the interior joint. The displacement reached the maximum value at 7.714 s, and the base shear force of the structure was 60.93 kN and the peak displacement of the girder was 11.96 mm at that moment. On the whole, the structure was fully elastic under the action of the frequent earthquake of 8-intensity (70 gal), which satisfied the fortification objectives of “no damage to minor earthquake”. When the PGA increased to 400 gal (equivalent to the rare earthquake of 8-intensity), no obvious plastic deformation and damage appeared on the frame, so it achieved the

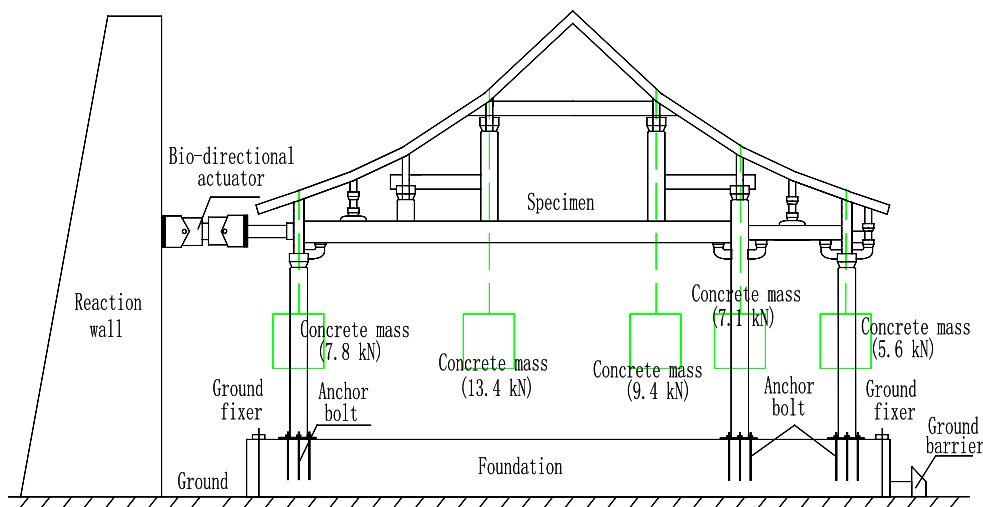


Fig. 6 Test setup

principle of “no collapse to rare earthquake.” Even under Wenchuan waves with the PGA of 620 gal (equivalent to a 9-intensity rare earthquakes), only some individual members yielded (Fig. 7), detected by the strain gauges values, and the integral performance was good, indicating that the structure has the ability to resist earthquakes beyond the local fortification standard and the TSBs have a good seismic performance.

3.2 Hysteretic Characteristics

Figure 8 shows the hysteresis curves of the base shear versus girder displacement in the PDTs. In order to make the graphs easier to compare with each other, the axis scale and interval were set the same. It can be seen from the figures that the hysteresis curves are not identical under the same PGA with different seismic wave, which indicates that the spectral characteristics of different seismic waves have a great influence on the seismic response of the structure. The structural response to Lanzhou wave is the smallest, while that of Wenchuan wave is the most obvious. With the excitation of the PGA of 70, 200 and 400 gal, the hysteresis curve cycled along a straight line basically. When the load reduced to zero, no residual deformation appeared, and the steel frame still worked in elastic state. With the increase of the PGA of seismic wave, the shear versus displacement responses of steel frame becomes more obvious, and the area surrounded by hysteresis loops increases gradually, and the energy consumption of structure gradually increases. When subjected to 620 gal Wenchuan wave, the hysteresis curve has residual deformation to a certain extent, and the structure enters into the elastic–plastic stage. The reason is that the yielding occurrence of the structural member increases the structural energy dissipation, but no obvious pinching phenomenon appears, which indicates that TSB possess high



Fig. 7 Yielding phenomenon

stiffness and excellent bearing capacity under the rare earthquakes of 9-intensity.

3.3 Energy Dissipation Capacity

Energy dissipation is the ability to absorb energy when seismic waves are input. The cumulative hysteretic energy is calculated by the following formula (Zhang et al. 2011):

$$E = \sum_{i=0}^n \frac{1}{2} (F_i + F_{i+1})(X_{i+1} - X_i) \quad (1)$$

where: F_{i+1} and F_i are the restoring force of $(i + 1)$ th point and the i th point, respectively, X_{i+1} and X_i are the corresponding displacements. Figure 9a shows the energy dissipation comparison of the structure under the same PGA but different types of seismic waves. It can be found that the various waveforms with different spectral characteristics lead to the different energy dissipation capacity of the structure. The hysteretic energy dissipation of the model structure subjected to Wenchuan wave is shown in Fig. 9b. With the excitation of 70 and 200 gal seismic waves, the cumulative hysteretic energy dissipation is relatively small, which demonstrates that the elastic strain energy takes the most of the entire energy consumption. Due to the randomness of the earthquake wave, the structural energy absorption increases when the input PGA increases, on the contrary, the energy dissipation decreases when the input acceleration of seismic wave decreases, which results in a wave-shape of the energy dissipation curve. With the increase of the input PGA, the energy consumption of the structure increases gradually. Under the action of the rare earthquakes of 9-intensity, the energy dissipation of the structure is about three times more than that of the 8-intensity rare earthquakes, which shows that the energy consumption increase non-linearly with the amplitude of the seismic waves increments. It can be seen from the experimental phenomena that no crack phenomenon occurred at this time, which means that TSB can not only resist the earthquake of 9-intensity, but also has high safety stock.

3.4 Acceleration and Displacement Response

Figure 10 is the acceleration time-history curves at the girder level of various loading condition. It can be seen from Fig. 10a that under different seismic waves, the structural acceleration response curve is basically consistent with the seismic waveform, but the structural response acceleration and the original waveform do not reach the extremes at the same time. The structural peak accelerations of El Centro wave, Lanzhou wave and Wenchuan wave occur at 1.484, 3.514 and 8.666 s, respectively. When the 200 gal peak acceleration wave is applied to the structure, the

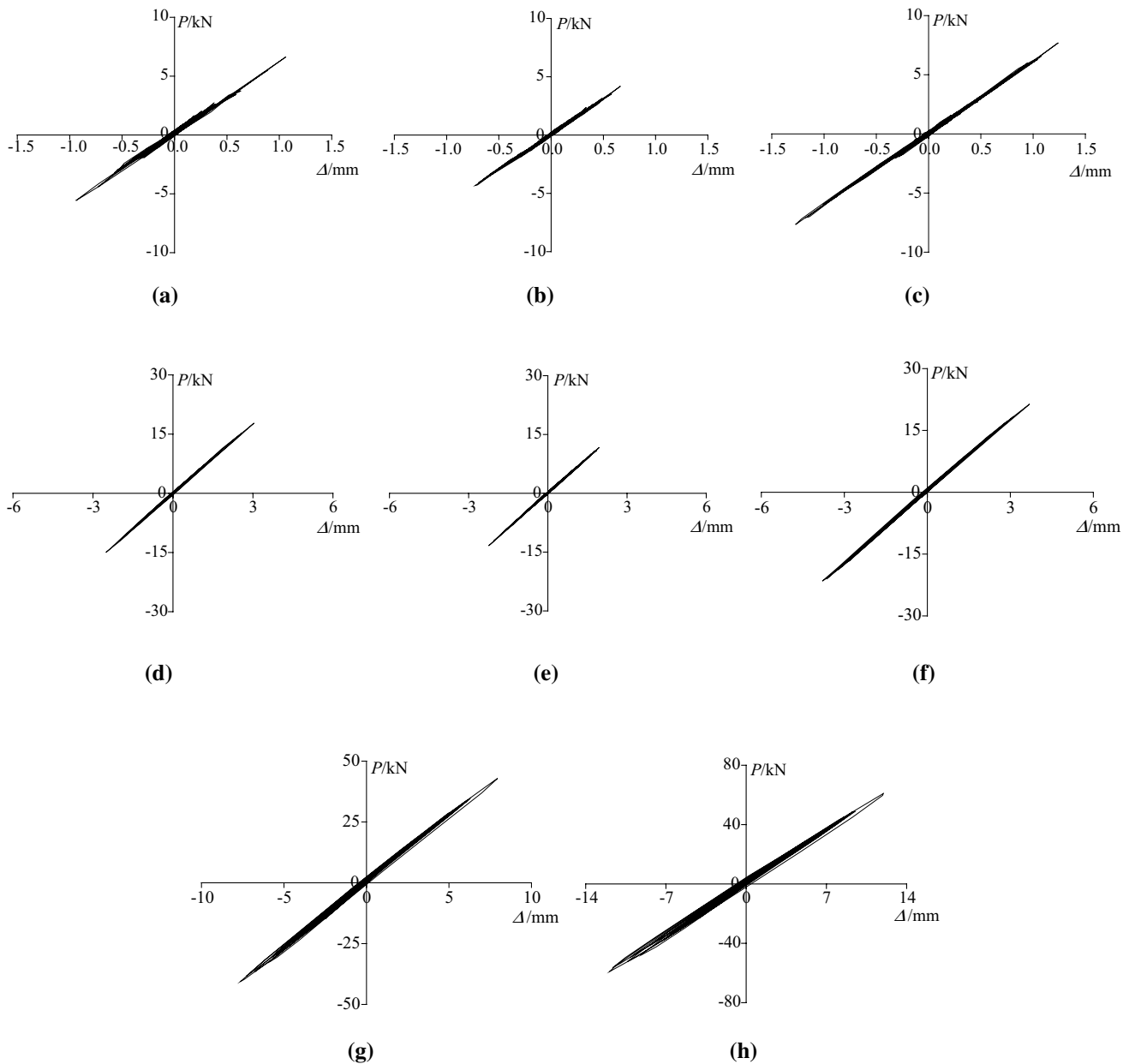


Fig. 8 Hysteretic loops. **a** Test No. 1 (70 gal El Centro). **b** Test No. 2 (70 gal Lanzhou). **c** Test No. 3 (70 gal Wenchuan). **d** Test No. 4 (200 gal El Centro). **e** Test No. 5 (200 gal Lanzhou). **f** Test No. 6 (200 gal Wenchuan). **g** Test No. 7 (400 gal Wenchuan). **h** Test No. 8 (620 gal Wenchuan)

maximum structural accelerations under El Centro wave, Lanzhou wave and Wenchuan wave occur at 1.778, 2.002 and 7.798 s. And the structural peak acceleration response is 407.1, 311.8 and 452.8 gal, respectively. The dynamic structural response of the Wenchuan wave, whose frequency is the closest to the structural fundamental frequency, is the most obvious, which indicates that the spectral response has a significant effect on the acceleration response of the structure. In addition, from Fig. 10b, the structural acceleration response of the structure increases with the increase of the input acceleration peak under the same seismic wave. With

the excitation of Wenchuan wave with 70, 200, 400 gal PGA, the structure is in an elastic working state, the time history curve and the original wave changing trend are basically the same. However, with the input acceleration peak increasing, the occurring time of structural peak response is slightly behind the peak moment of the original wave under the 620 gal Wenchuan wave, that is, the time-history curve changes from dense to sparse, which is because some components have reached the yield state, the structural stiffness decreases and the frequency also change with that, which affects the occurring time of the structural acceleration peak response.

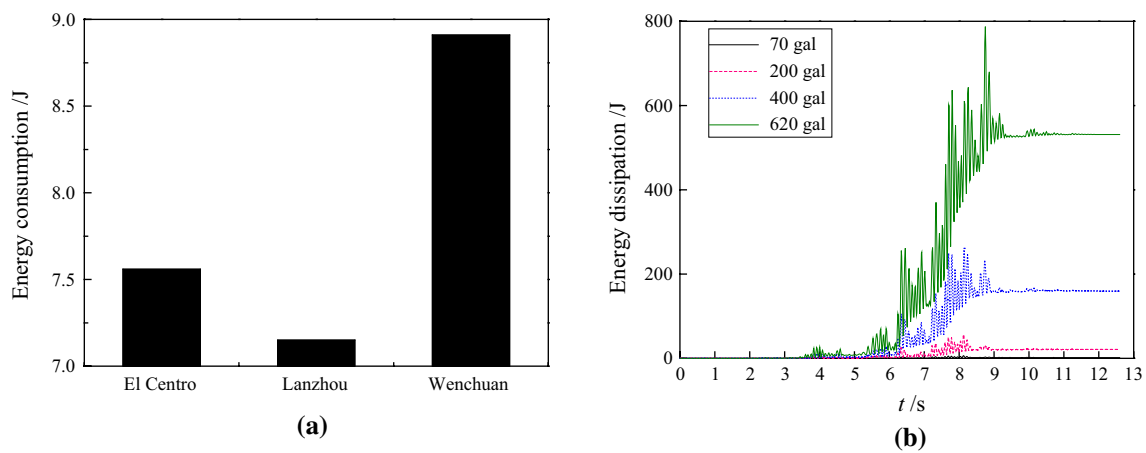


Fig. 9 Energy dissipation. **a** Under different waves. **b** Subjected to various acceleration peak

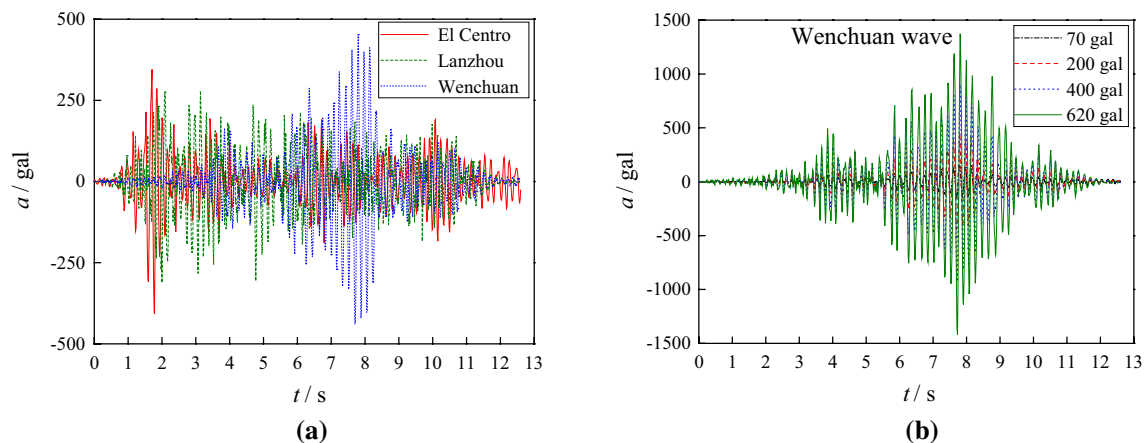


Fig. 10 Acceleration time-history curves. **a** 200 gal PGA. **b** Different PGA

The displacement time-history curves at the girder level of various loading condition are shown in Fig. 11. It can be drawn from the figures that when the input acceleration is relatively small, the displacement response of the whole model is not significant. The shape of structural displacement curve under different seismic wave excitation is about the same as that of the original wave. With the increase of PGA, the displacement response of the structure increase as well. When the seismic wave with peak acceleration of 200 gal is applied, the structural displacement response of Wenchuan wave, El Centro wave and Lanzhou wave are 3.795, 3.041, and 2.242 mm, respectively. The reason is that Wenchuan wave’s frequency is closest with the natural frequency of the specimen, and the difference between Lanzhou and the structural frequency is relatively large. In addition, the moment of maximum displacement response is not exactly the same as that of the input PGA. Figure 11 shows that the structural peak response postponed at the excitation of 620 gal wave, indicating that the structural damage leads

to the change of the stiffness, which makes the displacement response change obviously with the increase of PGA of seismic wave.

Table 5 shows the change of the interlayer displacement angle under Wenchuan wave. It can be seen that the maximum displacement angle of the structure is 1/1903 under the action of 8-degree frequent earthquake, which satisfies the displacement limit of the multilayer steel structure which is 1/250 in GB50011-2010. The displacement of the structure is 11.962 mm and the corresponding displacement angle is 1/203 when subjected to 9-degree rare earthquake, which can meet the requirement of plastic layer displacement angle of 1/50 in the current seismic code, indicating that the TSB has a good deformability.

3.5 Bearing Capacity and Stiffness

Based on the structural shear force versus top displacement curve subjected to Wenchuan wave, the backbone

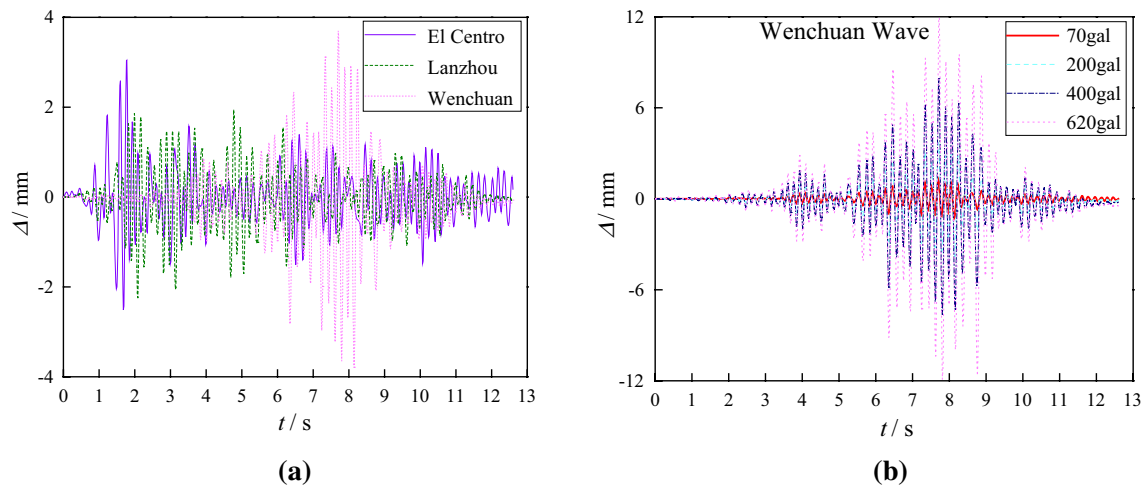


Fig. 11 Displacement time-history curves. **a** 200 gal PGA. **b** Different PGA

Table 5 Interstory displacement

Input acceleration peak, \ddot{x}_g (gal)	70	200	400	620
Interstory drift ratio, θ	1/1903	1/683	1/305	1/203

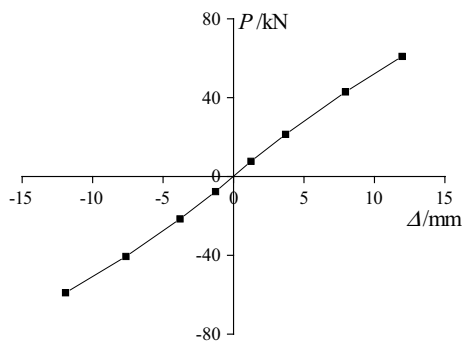


Fig. 12 Backbone curve

curve of the structure is obtained by connecting the maximum force point in the positive and negative directions under each working condition (Bai et al. 2011), as shown in Fig. 12. It can be found that with the increase of the peak acceleration of the input seismic wave, the structural displacement response increases and the bearing capacity of the structure increases continuously. With the 9-intensity rare earthquake (620 gal), the backbone curve still does not enter the descending section. The maximum interlayer displacement ratio of the structure is 1/203, which indicates that the TSB has good bearing capacity and high safety stock.

The stiffness degradation issue is an important part of the seismic performance and seismic calculation of this kind of structure. For the quasi-dynamic test with actual seismic

waves, the structural stiffness takes the mean stiffness in both directions, that is, the structural stiffness K_i takes the ratio of maximum base shear (sum of two directions) to corresponding displacement. The following equation can be obtained.

$$K_i = \frac{|+P_i| + |-P_i|}{|+\Delta_i| + |-\Delta_i|} \quad (2)$$

where, P_i and Δ_i are the maximum loads and corresponding displacements achieved at the i th loading, respectively. Table 6 shows the structural stiffness under different loading conditions. At the initial loading stage, there is a slight gap between the actuator and the specimen. Therefore, the structural stiffness measured at the loading condition 1 is slightly lower than that of the loading condition 2. To make the value more accurate, the initial stiffness K_0 is taken as 6.129 kN/mm.

The stiffness degradation law of the model can be found in Table 6. There is little change of stiffness basically before the loading condition of 5 (200 gal Lanzhou wave). When 200, 400 and 620 gal PGA of Wenchuan wave are applied, the overall structural stiffness degradation accelerated due to the cumulative damage. When the test is completed, the structural rigidity is still 81.9% of the initial stiffness, indicating that the integral stiffness is still high after 9-intensity of rare earthquakes.

4 FEM Modal Analysis

To further know the dynamic characteristics of TSB, three-dimensional nonlinear element model of the specimen has been constructed using SAP2000 finite element analysis software (Ren et al. 2004). The analytical model

Table 6 Variation of stiffness

Loading condition	Base shear, P (kN)	Top displacement, Δ (mm)	Stiffness, K (kN/mm)	Relative stiffness, K/K_0	Relative force, P/P_{\max}
1	6.108	1.002	6.096	0.995	0.102
2	4.260	0.695	6.129	1.000	0.071
3	7.683	1.257	6.112	0.997	0.128
4	16.682	2.776	6.009	0.980	0.278
5	12.536	2.093	5.989	0.977	0.209
6	21.462	3.746	5.729	0.935	0.358
7	41.742	7.790	5.358	0.874	0.696
8	59.976	11.941	5.023	0.819	1.000

is developed for obtaining the vibration performance and seismic behavior of this kind of structure. Thin shell element was chosen to simulate the whole structure, the ideal elastic–plastic hardening steel model was utilized and the material characteristics were identical with the coupon test values. The modal boundary condition was the same as the actual loading test, and keeping the model move in the loading plane to guarantee that no out-of plane buckling occurred. The non-linearity of the structure is realized by defining the plastic hinge, which are the default moment hinge of beams and the P-M-M hinge of columns, respectively. Due to the complexity of Dou-Gong components, shear and axial hinge are applied to them simultaneously. The analysis type is nonlinear direct integration and the P-Delta geometric nonlinearity is considered as well.

It is worth noting that because no loading step is considered during the modal analysis, the external vertical load should be added to the structural mass. Thus the mass source should contain the vertical load patterns. In addition, the theoretical frequency of the test specimen was calculated which was used to compare with the FEM results to guarantee the correctness the finite element model. The structural shapes of the first three modes are shown in Fig. 13. Table 7 displays the modal and calculated frequencies of the frame.

The vertical deformation of the second and third modes of the steel frame is larger than that of the first mode, but the horizontal deformation is obviously smaller than that of the first vibration mode. It is shown that the seismic response under the horizontal earthquake is mainly controlled by the first mode. The second and third modes are more complicated than the first vibration mode, and the local vibration phenomenon occurs in the main girder component.

The deformation of the steel frame structure is shear-type, and the deformation of the main span and the side span is basically coordinated and the cooperative working performance is great.

From the table, the FEM frequency is very close to that of the theoretical results, only showing 4.52% error, which validate the accuracy of the model. The structural response period is closest to the predominant period of Wenchuan wave, so the reaction of the specimen should be the most obvious subjected to Wenchuan wave, which matches the test phenomenon.

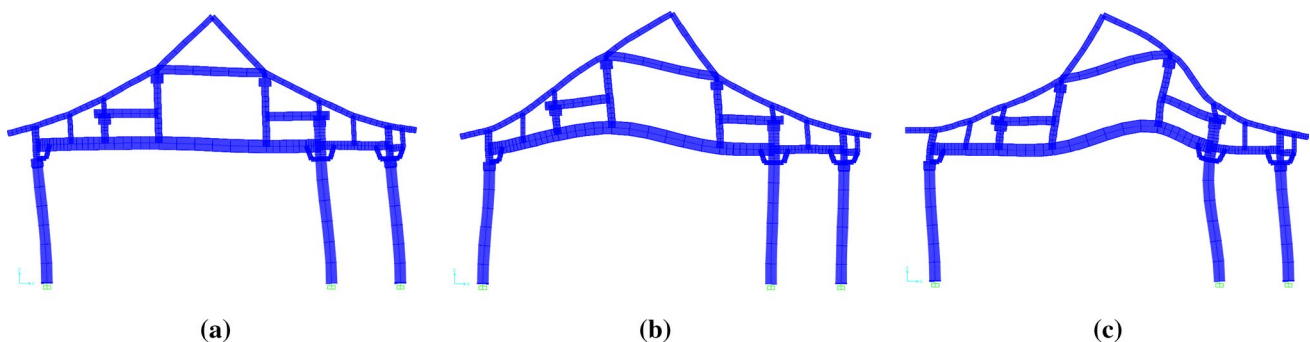
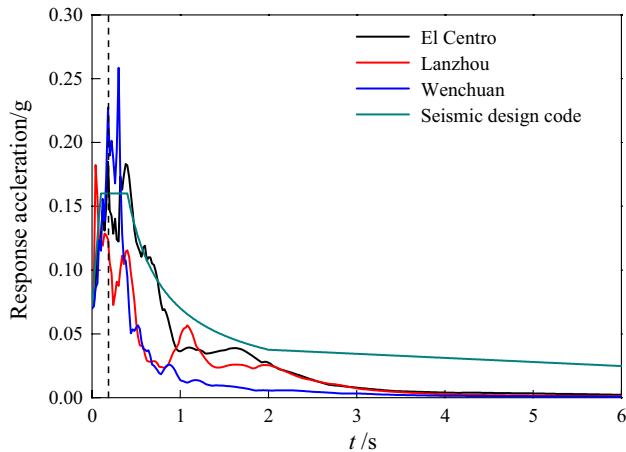
**Fig. 13** The modal shape. **a** First mode. **b** Second mode. **c** Third mode

Table 7 Structural vibration characteristics

Mode	Finite element model			Theoretical calculation	
	Circular frequency (rad)	Frequency (Hz)	Period (s)	Frequency (Hz)	Period (s)
1	33.85	5.39	0.185	5.65	0.177
2	92.38	14.71	0.068	–	–
3	173.39	27.61	0.036	–	–

**Fig. 14** Response acceleration spectrum

5 Time-History Analysis

5.1 Input Indexes Determination

As the specimen is a single-layer planar frame, all of the seismic waves are inputted in the structural plane along the lengthwise direction, the structural components mass and the vertical load are concentrated at the girder level, and the whole mass of the model is obtained, i.e. $[M] = 4863$ kg. In addition, according to the requirements of Chinese seismic design specifications, the damping ratio ζ of multi-storey steel structure equals to 0.04.

The damping matrix $[C]$ amounts to the linear combination of the stiffness matrix $[K]$ and the mass matrix $[M]$, which is Rayleigh damping, and the damping differences of different vibration modes are ignored.

The three tested seismic waves are transformed to acceleration spectrum curves, which are compared with the earthquake response spectrum in Chinese seismic design code, and shown in Fig. 14. The horizontal axis of the vertical dash line corresponds to the structural natural period. It can be seen that at the particular moment, the response acceleration spectrum of Wenchuan wave, El Centro wave and Lanzhou wave is 0.227, 0.185 and 0.124 g, respectively. The

response spectrum of Wenchuan wave is the most significant, which is consistent with the experimental results.

5.2 Verification of Tests

Considering the length of the paper, only the results of 200 and 620 gal PGA are shown hereby. Figure 15 shows the experimental and FEM time-history curves of the specimen. The simulation response curve demonstrates a good match with the experimental data, which verifies the correctness of Sap2000 model. Under the same loading condition, the reaction force of finite element software is a little larger than that of the test. Because of ignoring the Bauschinger effect in software, which is caused by simplifying the bilinear strain-hardening behavior of the steel, the FEM force response of the structure is more obvious. And damage phenomenon appeared in experiments which is neglected during simulation analysis. Moreover, the material constitutive model and damping is not exactly the same as real material. All of these reasons cause the deviation between test and simulation.

5.3 Parameter Analysis

In order to study the plastic response of TSB in depth, more severe earthquake waves are applied to test the specimen. The structural analyses are demonstrated as below.

5.3.1 Plastic Hinge Distribution

In Fig. 16, Point B represents yielding. Point Immediate Occupancy (IO) is when the building remains safe to occupy: any repairs are minor. Point Life Safety (LS) represents that the structure remains stable and has a significant reserve capacity: hazardous nonstructural damage is controlled. And the Collapse Prevention (CP) represents that the building remains standing, but only barely: any other damage or loss is acceptable.

When the peak input earthquake PGA is < 620 gal, no plastic hinge appears in TSB, which demonstrates the structural design is reasonable and economical. With the excitation of Wenchuan wave of 620 gal PGA, the western Dou-component of side span yields at 7.672 s. The plastic hinge distribution when subjected to 800 gal seismic wave is shown in Fig. 16a, three Dou-components enter

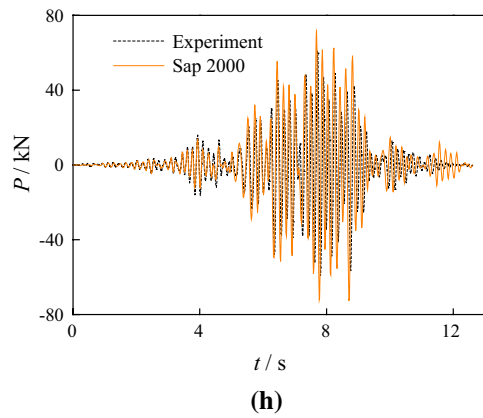
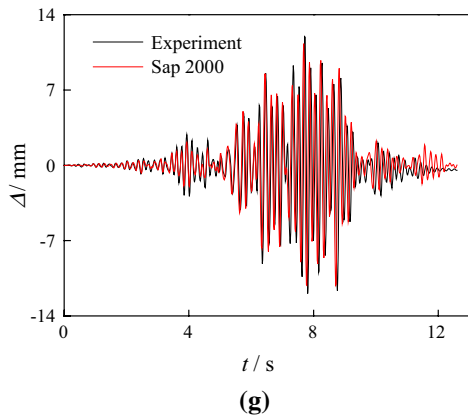
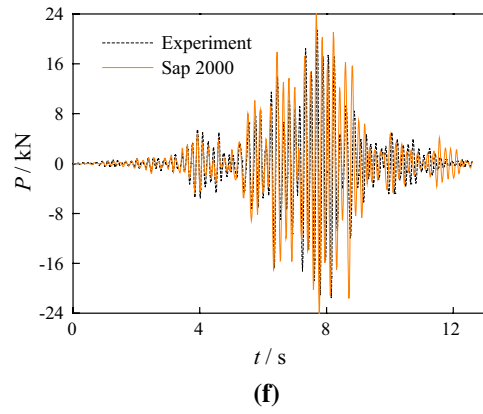
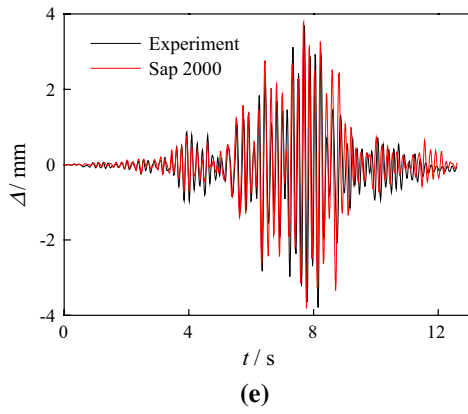
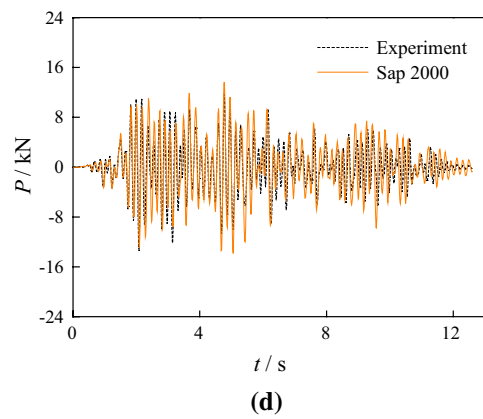
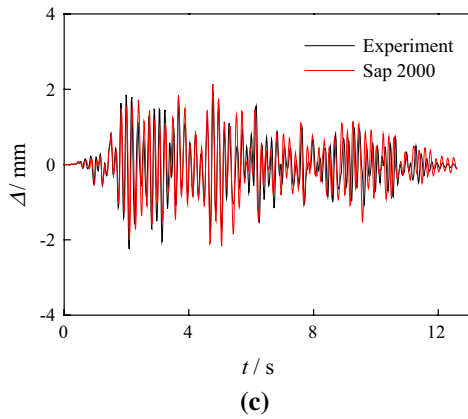
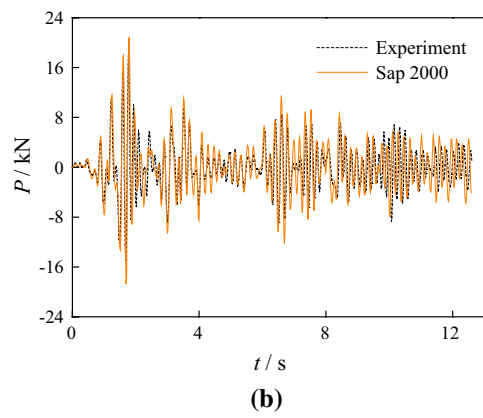
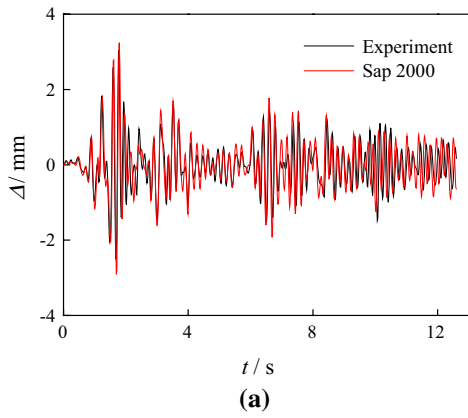


Fig. 15 Comparison of time-history curves. **a** Displacement time-history curve (El Centrol 200 gal). **b** Force time-history curve (El Centrol 200 gal). **c** Displacement time-history curve (Lanzhou 200 gal). **d** Force time-history curve (Lanzhou 200 gal). **e** Displacement time-history curve (Wenchuan 200 gal). **f** Force time-history curve (Wenchuan 200 gal). **g** Displacement time-history curve (Wenchuan 620 gal). **h** Force time-history curve (Wenchuan 620 gal)

the plastic stage, and exceed the Immediate Occupancy status, which shows that Dou-component plays as the first seismic line when subjected to the earthquake. The structural plastic hinge distribution under seismic wave whose PGA is 1000 gal is demonstrated in Fig. 16b. The yield phenomenon appears in more structural members, almost all Dou-components develop inelastic deformation. Gong-component at the side column of side span yields at 7.672 s, and it occurs before yielding of columns and beams. The Dou-component which first yield at the side span keeps in the Life Safety failure. From the above description, the Dou and Gong-components act as the first earthquake fortification line and dissipate most energy. After failure phenomenon occurred in these members, the structural members, beams and columns, will play a role in resisting the earthquake. In other words, the Dou and Gong-components delay the action time of other structural members, they protect the main structural members when subjected to earthquake. However, the middle column enters into plastic stage at 7.686 s, earlier than the beams yielding. The column base designing should be paid more attention and the strength be increased in practical engineering. Also, the stiffness ratio between the Dou-Gong and other structural members should be reasonable. If the Dou-Gong components are too strong, maybe it won't yield before other structural members, however, if they are too weak, it won't dissipate much energy, which is a little wasteful.

5.3.2 Characteristic Values with Hysteresis Analysis

The characteristic values under severe earthquakes are shown in Table 8. It can be seen that almost all the structural peak responses, including load, displacement and acceleration, occur during 7–8 s. The reason is that the maximum excitation of input wave is at 7.630 s (negative response) and 8.694 s (positive response). Because of the structural

damage accumulation, the most obvious reaction takes place in advance or delays a bit. Figure 17 illustrates the hysteresis curves of the structure. The hysteresis loop with 1000 gal PGA is fuller and the slope of the curve changes in the later loading period, which provides a good match with the plastic hinge research.

6 Conclusions

1. When the input seismic wave was no more than rare earthquake of 8-intensity, the traditional-style steel frame structure stayed in the elastic stage, which can meet the requirements of “No damage to minor earthquakes, no collapse to severe earthquakes”. As the PGA increased, the model damage accumulated and the energy dissipation increased. When the 9-intensity seismic wave was applied, the Dou-component at the side span yielded. The structural displacement angle met the requirement of the plastic displacement ratio limit, indicating that the traditional-style steel structure has a high bearing capacity and safety stock.
2. The model acceleration and displacement time-history response increases with the increase of the input PGA. Under the different seismic waves with the same PGA, the acceleration and the displacement time-history curves of the structure are quite different, which indicates that the spectral characteristic of the input seismic wave has a great influence on the seismic response of the structure.
3. The vertical deformation of the second and third modes of the steel frame is larger than that of the first modal shape, but the horizontal deformation is obviously smaller than that of the first vibration mode. The deformation of the steel frame structure is shear-type, and the FEM frequency is very close to that of the theoretical results.
4. According to time-history analysis, the reaction force value of finite element is a little larger than that of the test under the same loading condition. When the structure is subjected to more severe earthquake, the most obvious structural reaction takes place in advance or delays a bit. All Dou-components develop inelastic deformation and the middle column enters into plastic

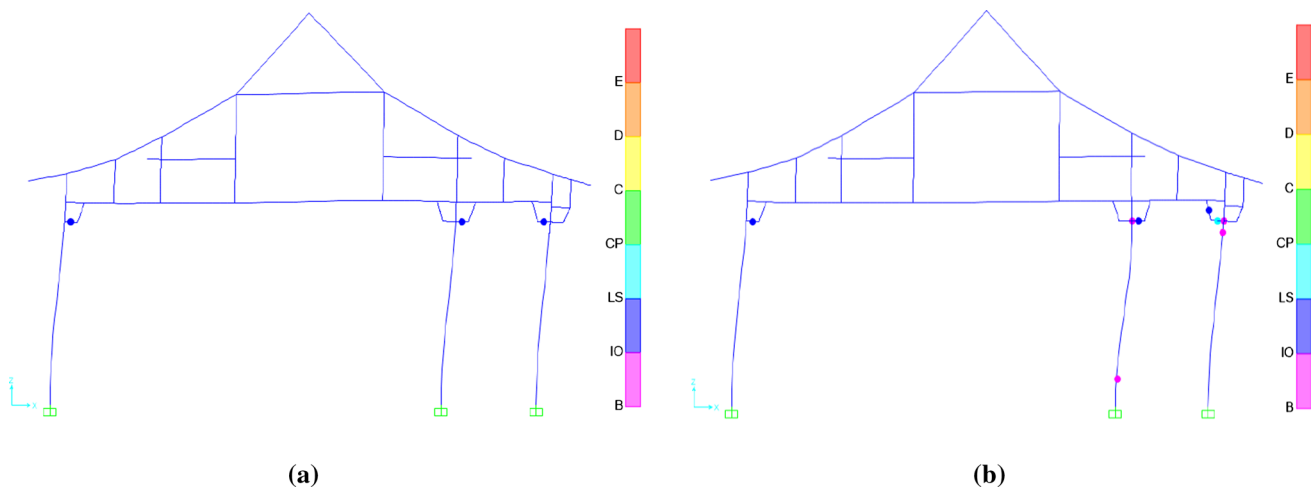


Fig. 16 Plastic hinge distribution. **a** Wenchuan 800 gal (PGA). **b** Wenchuan 1000 gal (PGA)

Table 8 Characteristic values under severe earthquakes

Seismic wave	Direction	Peak load		Peak displacement		Peak acceleration	
		Value (kN)	Time (s)	Value (mm)	Time (s)	Value (m/s ²)	Time (s)
Wenchuan wave 800 gal (PGA)	Positive	93.243	7.686	14.587	7.686	14.479	7.770
	Negative	-93.802	8.708	-14.388	7.784	-18.096	7.686
Wenchuan wave 1000 gal (PGA)	Positive	115.983	7.686	18.249	7.686	21.830	7.770
	Negative	-115.878	7.770	-17.816	7.784	-22.438	7.686

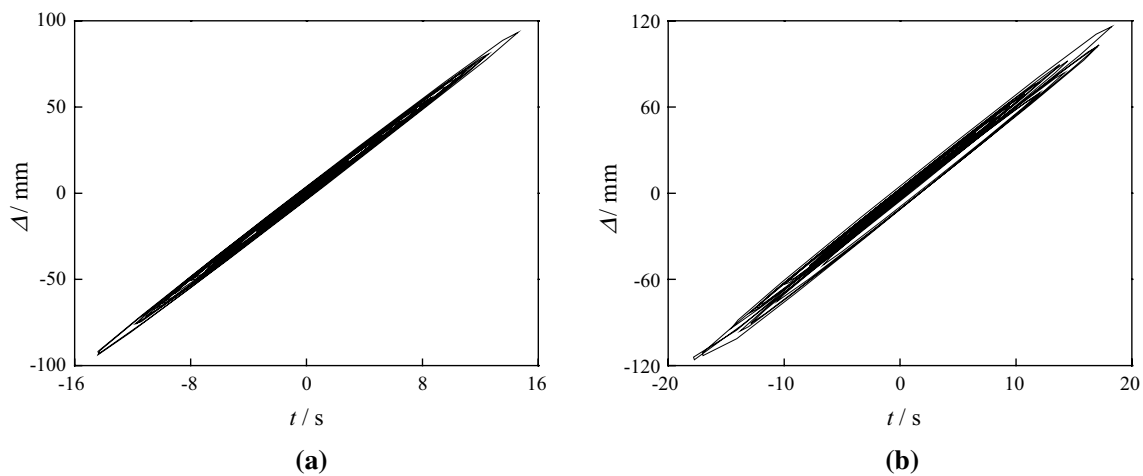


Fig. 17 Hysteresis curves. **a** Wenchuan 800 gal. **b** Wenchuan 1000 gal

stage earlier than the beams yielding when subjected to 1000 gal PGA Wenchuan wave.

(Grant No. CSCEC-2012-Z-16) and the Scientific Research Foundation of Outstanding Doctoral Dissertation of XAUAT (6040317006). Financial support from the China Scholarship Council for Liangjie Qi’s work at Virginia Tech, as a visiting scholar, is highly appreciated.

Acknowledgements This work was supported by the National Natural Science Foundation of China (Grant No. 51208411), the Technology Research Task of China State Construction Engineering Corporation

References

- Bai, G. L., Kang, L. G., Li, H. X., Li, X. W., & Zhao, C. L. (2011). Experimental study of the seismic performance of hybrid structure of SRC frame columns-RC disperse shear walls for large thermal power plants. *China Civil Engineering Journal*, 44(9), 20–26 (in Chinese).
- Baker, S. J. F., & Charlton, T. M. (1958). *A test on a two-storey single-bay portal structure*. London: British Welding Research Association.
- Fang, D. P., Iwasaki, S., Yu, M. H., Shen, Q. P., Miyamoto, Y., & Hikosaka, H. (2001). Ancient Chinese timber architecture. I: experimental study. *Journal of Structural Engineering*, 127(11), 1348–1357.
- GB50011-2010. (2010). *Code for seismic design of buildings*. Beijing: China Architecture & Building Press.
- Jan, T. S., Liu, M. W., & Kao, Y. C. (2004). An upper-bound pushover analysis procedure for estimating the seismic demands of high-rise buildings. *Engineering Structures*, 26(1), 117–128.
- Lauriola, M. P., & Sandhaas, C. (2006). Quasi-static and pseudo-dynamic tests on XLAM walls and buildings. *COST E29 international workshop on earthquake engineering on timber structures, Coimbra, Portugal*.
- Ren, W. X., Zhao, T., & Harik, I. E. (2004). Experimental and analytical modal analysis of steel arch bridge. *Journal of Structural Engineering*, 130(7), 1022–1031.
- Tian, Y. F. (2010). *Chinese imitated ancient building explanation*. Beijing: Chemical Industry Press (in Chinese).
- Tremblay, R., Archambault, M.-H., & Filiatrault, A. (2003). Seismic response of concentrically braced steel frames made with rectangular hollow bracing members. *Journal of Structural Engineering*, 129(12), 1626–1636.
- Tsai, K. C., Hsiao, P. C., Wang, K. J., Weng, Y. T., Lin, M. L., Lin, K. C., et al. (2008). Pseudo-dynamic tests of a full-scale CFT/BRB frame-Part I: specimen design, experiment and analysis. *Earthquake Engineering and Structural Dynamics*, 37(7), 1081–1098.
- Wodzicki, T. (2001). Natural factors affecting wood structure. *Wood Science and Technology*, 35(1–2), 5–26.
- Xue, J. Y., & Qi, L. J. (2016). Experimental studies on steel frame structures of traditional-style buildings. *Steel and Composite Structures*, 22(2), 235–255.
- Xue, J. Y., Wu, Z. J., Sui, Y., Ge, H. P., & Wu, K. (2016). Experimental study and numerical analysis on aseismic performance of steel double-beams-column interior-joints in traditional style building. *Engineering Mechanics*, 33(5), 97–105 (in Chinese).
- Xue, J. Y., Wu, Z. J., Sui, Y., & Liu, Z. Q. (2015). Experimental study on seismic performance of steel double-beams column exterior joints in antique style building. *Journal of Building Structures*, 36(3), 80–89 (in Chinese).
- Yang, Y., Liu, R. Y., Xue, Y. C., & Li, H. (2017). Experimental study on seismic performance of reinforced concrete frames retrofitted with eccentric buckling-restrained braces (BRBs). *Earthquakes and Structures*, 12(1), 79–89.
- Zhang, X. C., Xue, J. Y., Zhao, H. T., & Sui, Y. (2011). Experimental study on Chinese ancient timber-frame building by shaking table test. *Structural Engineering and Mechanics*, 40(4), 453–469.
- Zheng, S. S. (2000). Analogical ratio between scale models with less ballast and their prototypes under shaking table test. *Industrial Construction*, 30(3), 35–39 (in Chinese).